Int. J. Electrochem. Sci., 10 **(2015)** 8531 - 8548

International Journal of
ELECTROCHEMICAL
SCIENCE
www.electrochemsci.org

Investigation of the Electrocatalytic Properties of Spherical Palladium Nanoparticles and Palladium(100)iridium Bimetallic Nanocomposites towards Ammonia Electrooxidation on Pt Electrodes

Nolubabalo Matinise, Fanelwa Rachel Ajayi, Chinwe O. Ikpo[*]*, Njagi Njomo, Natasha Ross, Priscilla Baker and Emmanuel I. Iwuoha*

SensorLab, Department of Chemistry, University of the Western Cape, Robert Sobukwe Road, Bellville 7535, Cape Town, South Africa
*E-mail: cikpo@uwc.ac.za

Received: 8 July 2015 / *Accepted:* 6 August 2015 / *Published:* 26 August 2015

The electrocatalytic properties of cubic palladium-iridium {Pd(100)Ir} bimetallic nanocomposite and spherical nanoparticles {Pd NPs} towards the electrochemical oxidation of ammonia were investigated in sodium hydroxide on platinum electrode. Interrogation of their electrocatalytic properties through cyclic and square wave voltammetric techniques (CV and SWV)) revealed that the bimetallic nanocomposite {Pd(100)Ir} has better conductivity and higher catalytic activity as evidenced by the maximum current density reached for NH_3 oxidation at 1.9838 x 10^{-4} A with a decreased onset potential. The Pd NPs gave a maximum catalytic current value of 1.45 x 10^{-4} A. This was further validated by the results from electrochemical impedance spectroscopy (EIS) where the bimetallic nanocomposite gave charge transfer and solution resistance values of 96.35 Ω and 137.9 Ω, respectively with the nanoparticles exhibiting higher resistances at 670.6 and 189.5 Ω. These results confirm that facile interfacial electron transfer processes occur on the Pt/Pd(100)Ir electrode during the electrocatalytic ammonia oxidation and were made possible by the synergistic effect of the bimetallic palladium and iridium in the nanocomposite which causes a weakening of the adsorption strength of poisonous adsorbed nitrogen (N_{ads}) during the electrooxidation process.

Keywords: Bimetallic nanocomposite, electrochemical properties, ammonia electrocatalyst, chemical synthesis, electrochemical impedance spectroscopy.

1. INTRODUCTION

The electrochemical oxidation of ammonia has been expansively studied by many scientist due to its wide applicability in analytical chemistry, energy conversion processes for the production of

hydrogen in fuel cell; the remediation of ammonia-contaminated waste waters and indirect ammonia fuel cell [1-3]. The main advantage of the electrooxidation of ammonia is that no chemicals or bacteria are required but only electrical energy is consumed for the elimination of pollutants [4]. The mechanism of ammonia electrooxidation involves dehydrogenation of adsorbed ammonia and formation of nitrogen and hydrogen as final products [5].The process of electrooxidation of ammonia is very sluggish and hence requires the use of catalysts to speed up the reaction [6]. Researchers are saddled with the task of designing and developing suitable and efficient catalysts for ammonia oxidation. Most studies have considered the use of transition metals for the electrochemical oxidation of ammonia. Principally, in association with application in electrochemical fuel cells, environmental catalysis and electrochemical detection of ammonia, platinum was found to be the most active catalyst [7]. It is well known that platinum is very expensive and it easily gets deactivated by adsorbed nitrogen (N_{ads}) thus forcing researchers to focus on developing better and stable catalyst such as bi and multi metallic catalysts. Many researchers have reported their findings on the study of the electrochemical behaviour of ammonia on several electrodes such as Pt, Ru, Pd, Ir, Au, Pt–Me binary alloys and metal oxides (RuO_2, IrO_2, and PbO_2) in order to find the best electrocatalyst for ammonia electrooxidation [4, 8]. Platinum and its alloys always show good capability to dehydrogenate ammonia with a sufficiently low affinity to produce adsorbed nitrogen atoms and therefore it was concluded that platinum and its alloys are the best active catalyst towards electro- oxidation of ammonia. They have the ability to electrochemically convert ammonia to nitrogen in comparison with other metals [9-11]. In this study, we describe the synthesis and characterization of cubic Pd-Ir bimetallic nanocomposite and spherical Pd nanoparticles; and then compare their electrocatalytic activity towards electrooxidation of ammonia. Palladium has been used as a catalyst in many coupling reactions. Pd has properties similar to those of platinum. Therefore, Pd is considered as a promising electrocatalyst for electrochemical applications [12,13].

2. EXPERIMENTAL

Palladium(II)chloride ($PdCl_2$), iridium(II)chloride ($IrCl_2$), ethanol, poly(vinyl pyrrolidine) (PVP), L-ascorbic acid, potassium bromide (KBr-), potassium chloride (KCl-), and ammonium hydroxide (NH_4OH) were all purchased from Sigma-Aldrich and used for the chemical synthesis of nanomaterials. All chemicals are analytical reagent grade and were used without further purification. Deionized water (18.2 MΩ cm) ultra-purified water with a Milli-QTM water purification system (Millipore) was used throughout the experiments for aqueous solution preparation. Analytical grade argon gas purchased from Afrox Company, South Africa was used to degas the solutions for the electrochemical studies.

Pd(100)Ir nanomaterial was synthesized through a modified aqueous phase approach [14]: sequentially, the nanomaterials were prepared by mixing two solutions, one containing 8 mL of an aqueous solution of 0.1 M PVP and L-ascorbic acid, another one containing 20 mL solution of 0.1 M KBr and KCl. The solution containing PVP and ascorbic acid was used as a selective reducing and capping agent for the Pd-Ir shell. The solution containing KBr and KCl was used for controlling the

size and shape of the nanomaterial. The mixture was then placed on a magnetic stirrer and pre-heated at 80 °C for 5 min. To this mixture, 3 mL of an aqueous solution containing 0.1 M $PdCl_2$ and $IrCl_2$ (1:1) was added drop-wise using a drop pipette. Stirring continued at 80 °C for 1.5 h, after which black precipitation of Pd(100)Ir was formed from the reaction vessel. The nanomaterial was removed from the heating surface and cooled to room temperature. The product was centrifuged and washed with deionized water to remove all excess PVP. Palladium nanoparticles were synthesized using sodium citrate as the selective capping agent to control the growth of the nanoparticles while hydrazine and KOH were used as reducing agents [15]. Precisely, 50 mM $PdCl_2$ was dissolved in a cold 0.1 M sodium citrate solution which was purged with argon gas for 20 min. The solution was stirred with a magnetic stirrer at a mixing rate of 1125 rpm for 30 min at room temperature. To this solution, 30 µL of hydrazine and 200 µL of 9 M KOH were added. Thereafter, the mixture was continuously stirred for another 15 min until dark brown precipitates of the Pd NPs were formed. The nanoparticles were centrifuged and subsequently washed with deionized water.

BAS 100W integrated automated electrochemical workstation from Bio Analytical Systems (BAS, West Lafayette, IN) was used to perform all electrochemical experiments controlled by a computer and a conventional three-electrode system consisting of a 0.071 cm^2 platinum (Pt) disk electrode as the working electrode, a platinum wire as the auxiliary electrode and Ag/AgCl reference electrode with a 3 M NaCl salt bridge solution. Cyclic voltammetry (CV) measurements were carried out at a potential window of -1000 mV (initial potential) to + 600 mV at various scan rates. For square wave voltammetry (SWV), the experimental conditions were; amplitude of 25 mV, a frequency of 15 Hz and various scan rates were applied. All experimental solutions were de-oxygenated by bubbling with high purity argon gas for 15 min and blanketed with argon during all measurements and at room temperature (25 ºC). Electrochemical impedance spectroscopy (EIS) analysis was recorded with Zahner IM6ex Germany from Bio Analytical systems, BAS, US in three-electrode electrochemical cell.

Alumina micro-polish (1.0, 0.3 and 0.05 mm alumina slurries) and polishing pads (Buehler, IL, USA) were used for polishing the electrode surfaces before and after measurements

High transmission electron microscope (HRTEM) images were acquired using a Philips Technai TEM instrument operated at an accelerating voltage of 120 kV. HRTEM samples were prepared by dispersing the synthesized nanomaterials in ethanol and drop-casting on carbon coated copper grid. The solvent was allowed to dry at room temperature for about 30 min prior to measurements. The elemental compositions of the samples were determined using Energy Dispersive X-ray Spectroscopy (EDX). UV/vis experiments were performed on a Nicolette Evolution 100 Spectrometer (Thermo Electron Co-operation, UK) with the samples dissolved in ethanol and placed in $3cm^3$ quartz cuvettes. The spectra were recorded in the region of 350 – 700 nm. Atomic force microscopy (AFM) was used to study the surface morphology of the nanomaterials.

2.1. Electrode preparation

10 µL of each of the nanomaterials solutions was diluted with 100 µL of deionized water and 3 µL of 5 % nafion. The nafion binds the nanomaterials to the surface of the platinum electrode. Cleaned

Pt electrode was dried with nitrogen before drop coating 5 μL of the nanomaterials onto the electrode surface. The modified platinum electrode was dried at room temperature for 2 h before being immersed into ammonia-free 0.1 M NaOH and 0.1 M NaOH solution containing ammonia.
Electrochemical experiments were performed in a three-cell assembly under nitrogen bubbling for 15 min and scanned at 50 mV/s.

3. RESULTS AND DISCUSSION

3.1 Characterization of Pd NPs and Pd(100)Ir

3.1.1 HRTEM and EDX analysis of Pd(100)Ir bimetallic nanocomposite

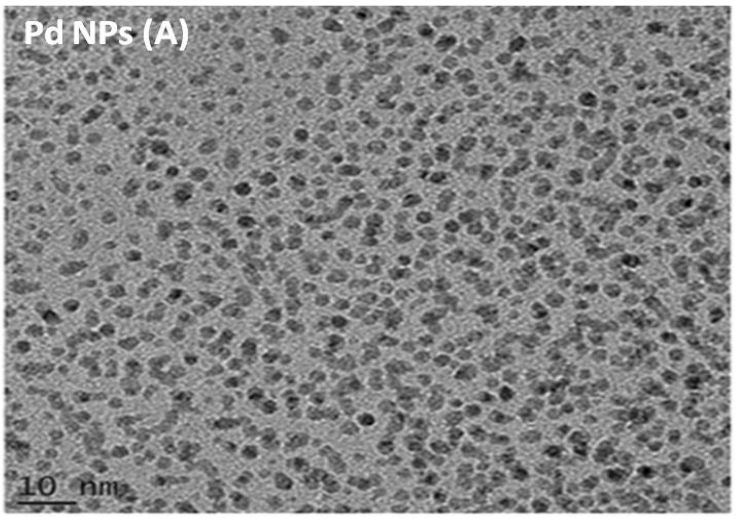

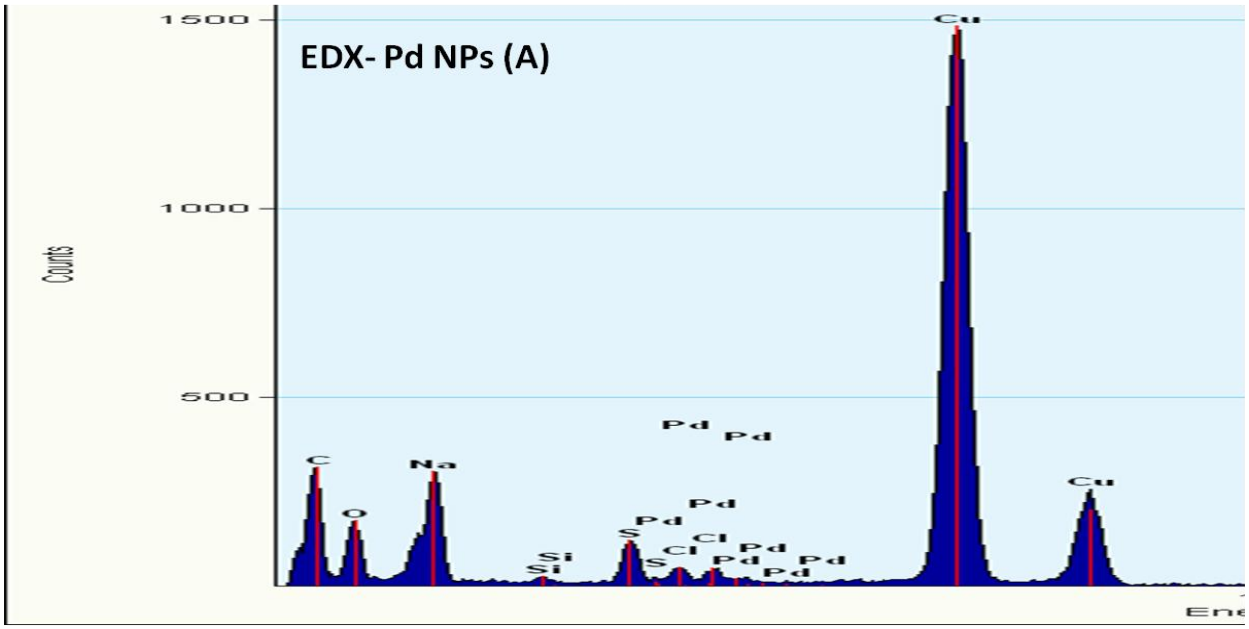

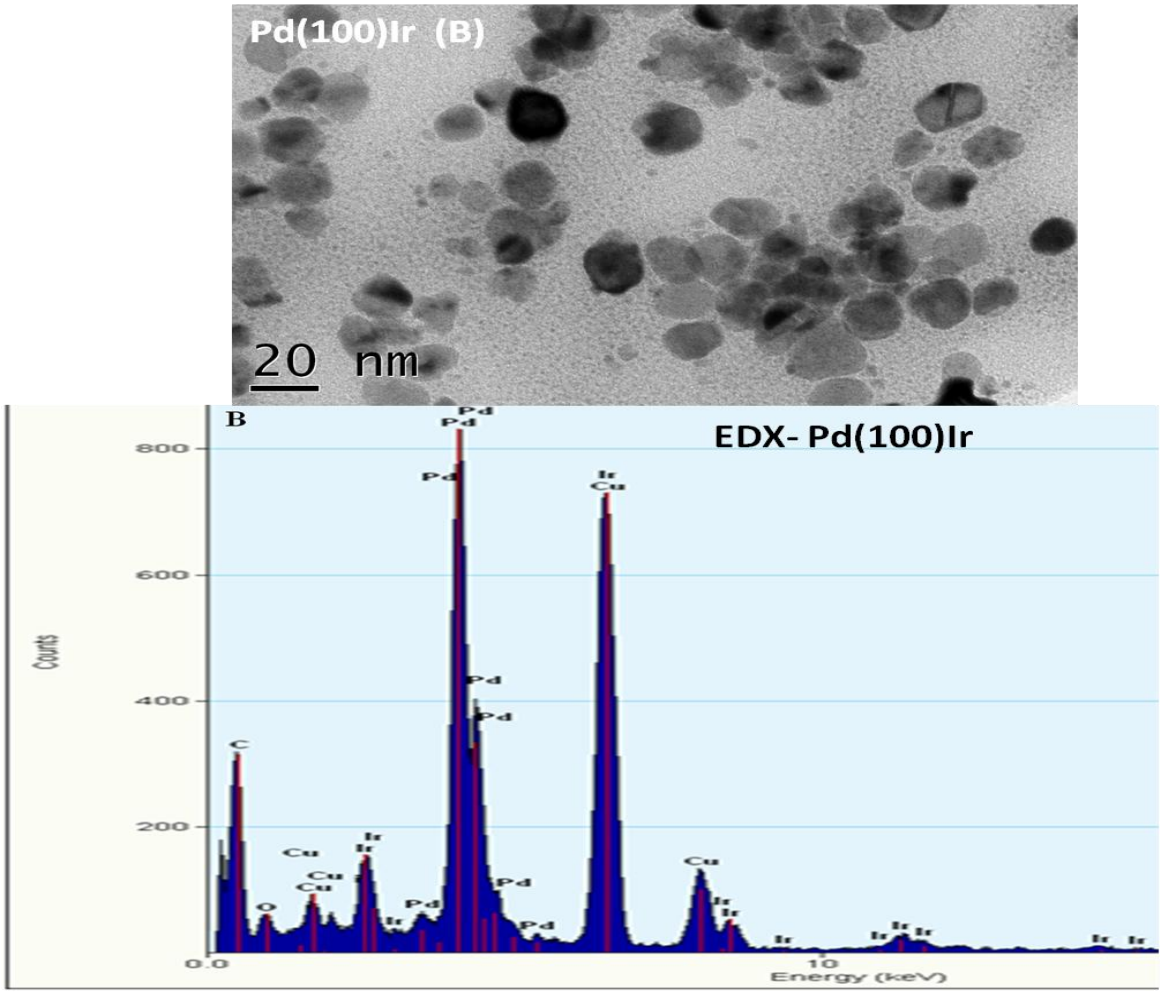

Figure 1. HRTEM image and EDX spectra of Pd NPs (A) Pd(100)Ir nanocomposites (B).

The HRTEM images in Fig. 1 reveal the morphology of the Pd NPs (A) and bimetallic nanocomposite {Pd(100)Ir} (B). Indicated here are well dispersed, uniformly distributed Pd NPs and Pd(100)Ir with particle sizes of about 2 and > 10 nm, respectively. The images revealed less agglomeration which is a fair indication that they have promising properties for electrochemical applications as they would render their high electrochemical active surface areas for better electronic and ionic transport. Energy-dispersive X-ray (EDX) analysis performed during the HRTEM observation gave evidence of the constituent elements in the synthesized nanomaterials. The EDX spectra in Fig. 1 (A and B) showed the optical absorption peaks close to 3; 11 and 13 keV which were due to the presence of Pd and Ir respectively. Carbon and oxygen peaks observed in Fig. 1 (B) near 1 keV, were due to the capping agent (PVP and ascorbic acid) while the Br peaks located near 2, 11.5 and 13 ekV were due to the reducing agent (KBr) used during the synthesis of the nanocomposites. The copper peaks shown close to 1.5, 8 and 9 keV were from the copper grid onto which the nanocomposites were drop-coated for HRTEM analyses.

3.2. Atomic force microscopy (AFM) analysis of monometallic nanoparticles {Pd NPs} and bimetallic nanocomposites{Pd(100)Ir}

Atomic force microscopy (AFM) was also performed to characterise the surface morphology and chemical composition of nanomaterials {Pd NPs and Pd(100)Ir}. Fig. 2 (A and B) shows the AFM images. It can be seen that for the 2-D image for each case, there is a uniform distribution of the nanomaterials. The 3-D images gave clear indications of the rough nature of the surfaces of the Pt electrodes illustrating that indeed these materials were attached. The surface features showed the Pd NPs to have a height distribution of 0-1.02 μm (Fig. 2 A) while the Pd(100)Ir showed a height distribution of 0-1.46 μm (Fig. 3.3 B).

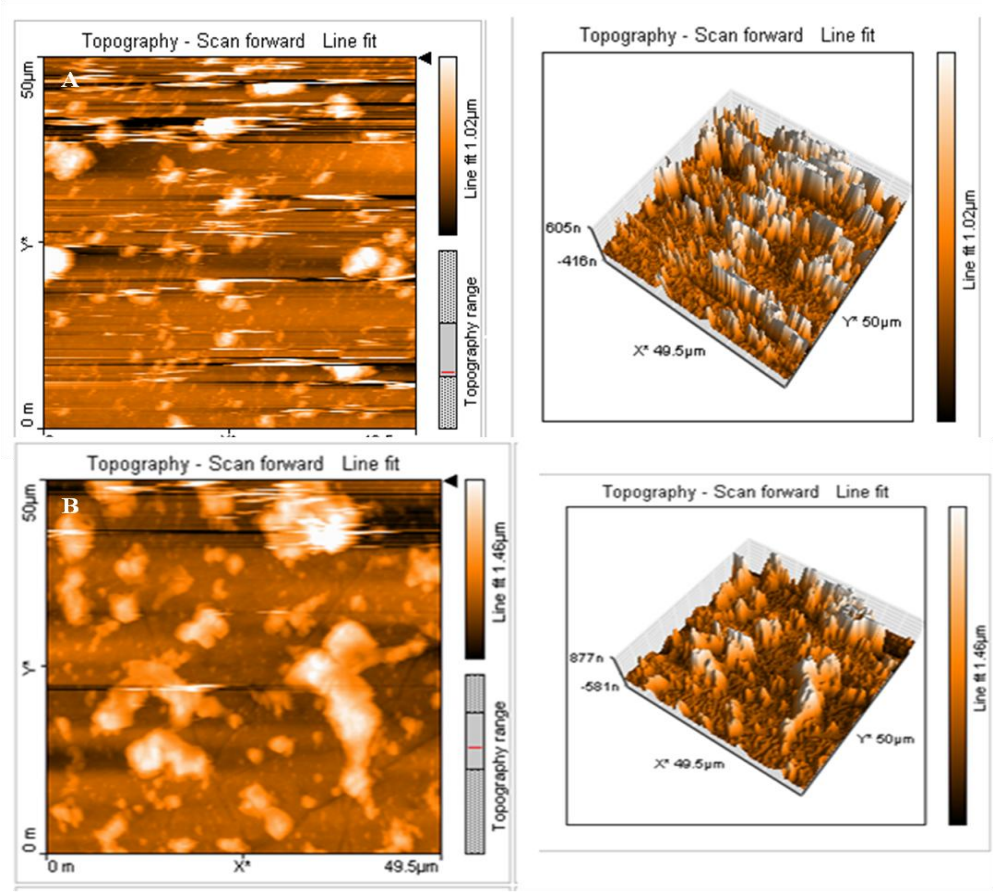

Figure 2. AFM images of Pt/Pd NPs (A) and Pt/Pd(100)Ir (B).

3.3 UV-vis analysis of monometallic nanoparticles {Pd NPs} and bimetallic nanocomposites {Pd(100)Ir}

UV-vis measurements were used to identify the reduction of Pd(II) ions to Pd nanoparticles. The UV-vis spectra of $PdCl_2$ (starting material), Pd NPs and Pd(100)Ir in ethanol are shown in Fig. 3. The UV–vis spectra of the reference sample $PdCl_2$ (Fig. 3 C) showed two absorption bands at 323 and 423 nm which correspond to metal transitions of Pd^{2+} ions in $PdCl_2$ [16,17]. However, for the reduced

samples (Figs. 3 (A and B)), the absorption peaks around 323 and 423 nm were entirely removed thus indicating the complete reduction of Pd(II) ions to Pd (0) [18].

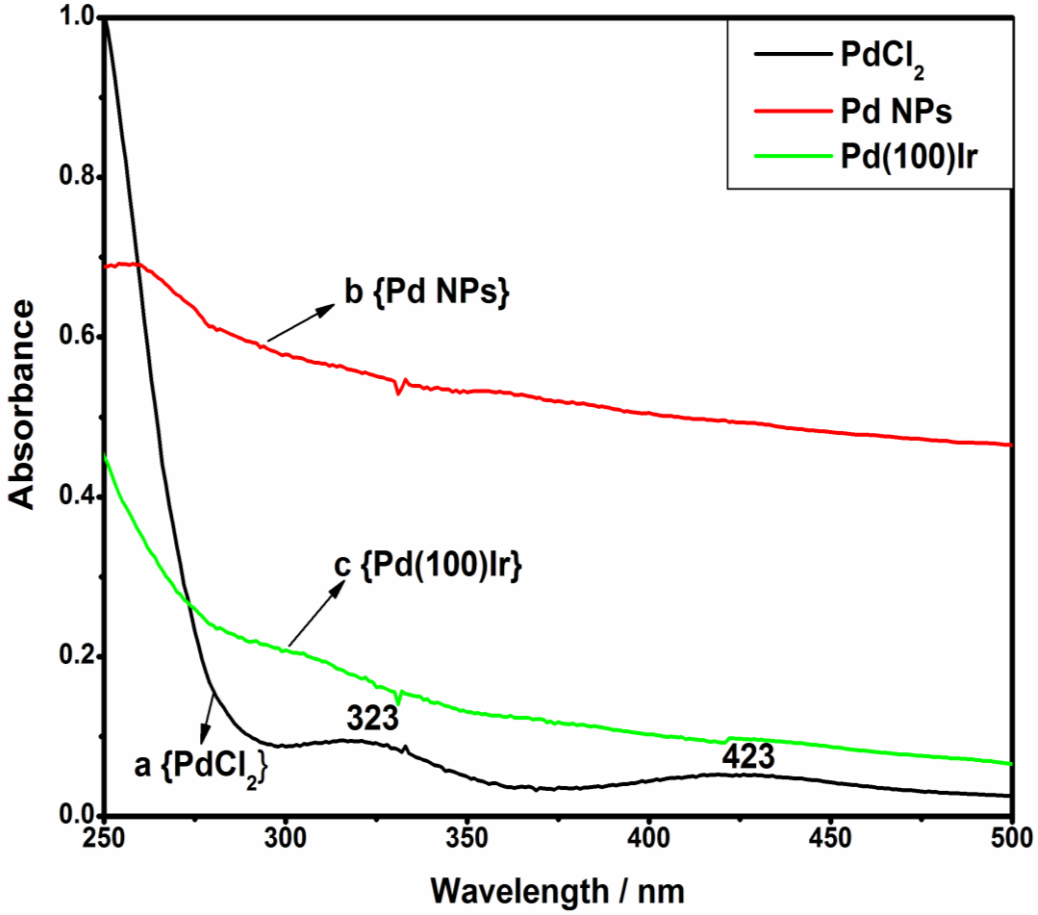

Figure 3. UV-vis spectrum of $PdCl_2$ (a), Pd NPs (b) and Pd(100)Ir (c).

3.4. Electrochemical study of Pd(100)Ir nanocomposites by voltammetric techniques

Voltammetric techniques (CV and SWV) were extensively used to evaluate the electrocatalytic properties of Pd NPs and Pd(1000)Ir films on platinum electrode surface by studying the reversibility of electron transfer. Typical voltammograms of Pd(100)Ir nanocomposite catalysts on Pt electrode are shown in Fig.4 (A and B), which were acquired at room temperature (25 °C) from -1000 to 600 mV vs. Ag/AgCl at a scan rate of 50 mV/s in argon- saturated 0.1 M NaOH solution. Three potential peaks were observed during the positive-going sweep which correspond to different electrochemical processes namely, the absorption and adsorption of hydrogen, the double layer charging and the surface oxide formation / reduction [19, 20]. These voltammograms revealed the well-known hydrogen adsorption/desorption peak (Peak I) at a potential range ≈ - 0.95 to ≈ - 0.60 V for the cathodic and anodic peaks [19, 20].

$$Pd(100)-H_{abs/ads}-Ir+OH^{-}\rightarrow Pd(100)Ir+H_2O+e^{-} \qquad (3.1\ a)$$

Peak II observed at ≈ 0.4 V indicates the formation of Pd(100)Ir-O on the platinum electrode.

$$Pd(100)-OH-Ir \rightarrow Pd(100)Ir-O+H^{-}+e^{-} \qquad (3.1\ b)$$

In the positive-going sweep, a strong reduction peak, (Peak III) observed at around ≈ -0.40 V can be attributed to the reduction of Pd(II) oxide into elemental Pd during the cathodic sweep [20].

$$Pd(100)Ir-O+2H^{+}+2e^{-} \rightarrow Pd(100)Ir+H_2O \qquad (3.1\ c)$$

Further characterization was carried out using SWV as shown in Fig. 4 (B) and the results compare well with those from the CV. This shows that the nanomaterials have good electrochemical activity and are considered as promising electrocatalysts for electrochemical applications.

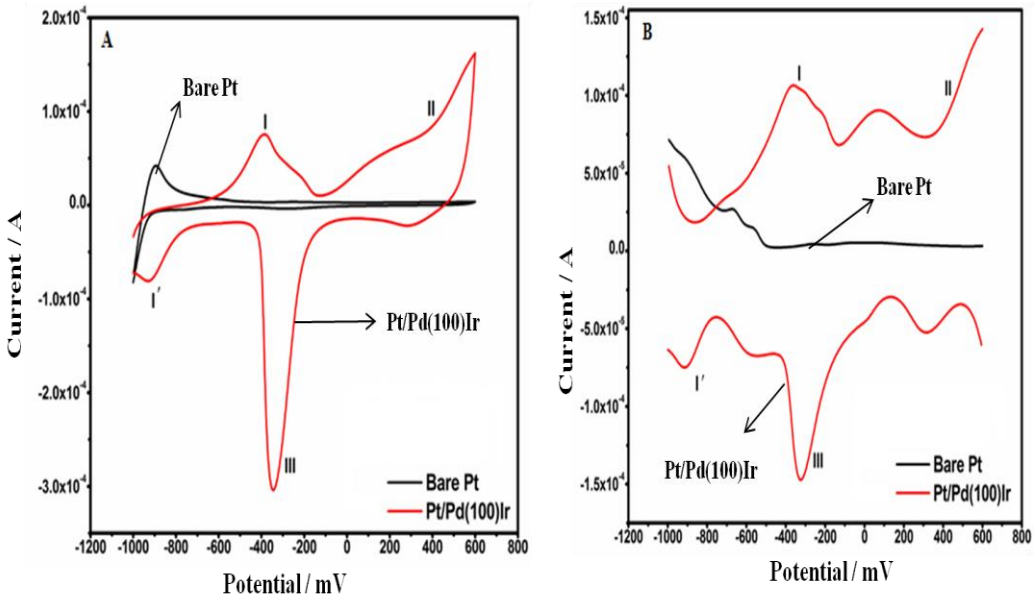

Figure 4. Electrochemical characterization {CV (A) and SWV (B)} of modified Pt electrode with Pd(100)Ir in 0.1 M NaOH at a scan rate 50 mV/s.

3.5. Comparison of monometallic Pd NPs and Pd(100)Ir nanocomposites

The bimetallic nanocomposite in Fig. 5 (A and B) showed a higher affinity for oxygenated species compared to the monometallic nanoparticles as evidenced by the peak potential shift on the PdO reduction and increase in peak current density (peak III) towards more negative potentials; thus indicating an enhanced electrochemical activity [21]. The higher peak current density suggests higher electrochemically active surface area for the bimetallic nanocomposite. The results confirm that the Pd(100)Ir has much higher electrocatalytic activity than the Pd NPs due to the synergistic effect of the two transition metals. The electrochemically active surface areas (EASAs) of the electrodes were calculated by determining the charge involved in the reduction of palladium (II) oxide into palladium metal. The EASA of the electrode was estimated using Equation 3.2.

$$EASA = Q/S \qquad (3.2)$$

where Q is the coulombic charge (in μC) and S is the proportionality constant (405 μC cm^{-2}) [20]. A theoretical charge value of 405 μC cm^{-2} is considered for the reduction of a PdO monolayer. The EASA of Pd(100)Ir and Pd NPs were calculated to be 80.20 and 50.54 cm^2 respectively. The enhanced electrocatalytic ability of the bimetallic nanocomposite {Pd(100)Ir} was proved by the

increased peak current density at peaks I, II and III when compared to monometallic nanoparticles {Pd NPs}. The high electrochemically active surface area and high electrocatalytic activity of bimetallic nanocomposite {Pd(100)Ir} indicate superior electrochemical performance over the monometallic palladium nanoparticles.

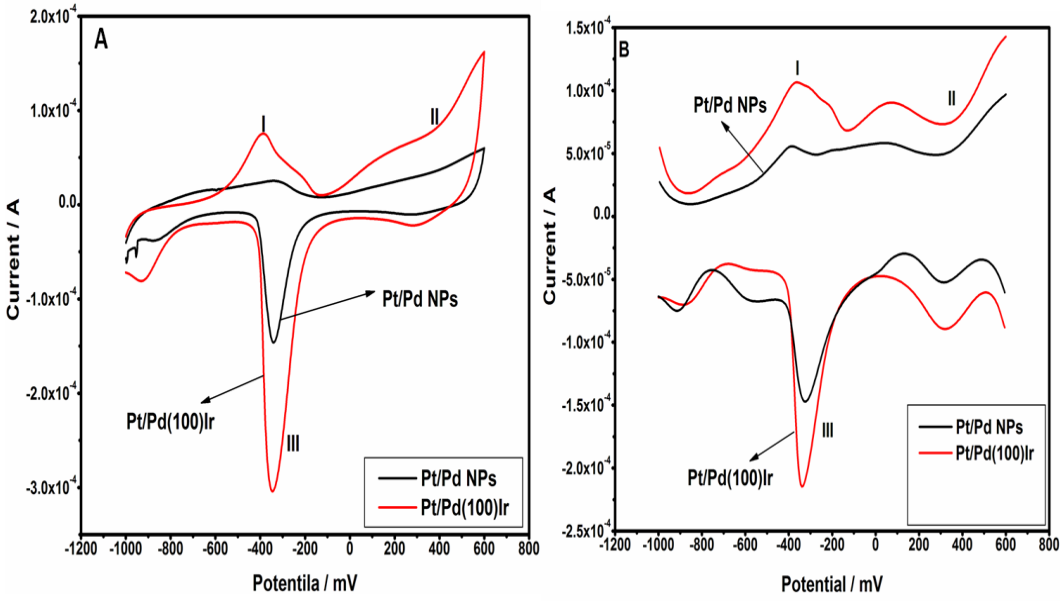

Figure 5. Electrochemical characterization {CV (A) and SWV (B)} of modified Pt electrode with Pd NPs and Pd(100)Ir in. 0.1 M NaOH at a scan rate 50 mV/s.

3.6 The effect of scan rate (v) on CV and SWV of Pd(100)Ir.

The effect of scan rate (v) on the electrochemistry of Pd(100)Ir nanocomposite was studied in 0.1M NaOH solution as observed in Fig 6 where the chosen scan rates were 10, 20, 30, 40,50, 60, 70, 80, 90, and 100 mV/s. The electrochemical performance of the material can be evaluated by observing the peak current density in the cathodic and anodic scan. The reduction peak current density of Pd(100)Ir showed an increase with increase in scan rate, whereas the potential revealed a slight shift to more negative values. The increase in peak current density as scan rate increases showed the stability of Pd(100)Ir nanocomposite on the electrode. It also illustrates that Pd(100)Ir nanocomposite is electro-active and diffusion takes place through the metal cavity [22]. The Randles-Sevčik plot exhibited an excellent linear graph with a correlation coefficient of 0.97135 ≈ 1, which indicates a diffusion controlled process at the Pt/Pd(100)Ir electrode and electrolyte interface. The diffusion coefficient, D was calculated using Randles-Sevčik Equation {Equation (3.3)}

$$I_p = \left(2.69\times10^5\right) n^{3/2} A D^{1/2} v^{1/2} C \qquad (3.3)$$

Where, I_p = current in amps, n = number of electrons transferred, A = Area of electrode in cm^2, D = diffusion coefficient in cm^2/s, F = Faraday constant in C mol^{-1}, C = concentration in mol/cm^3, v = scan rate in V/s.

The diffusion coefficient of the Pd(100)Ir ($5.864e^{-6}$ cm^2/s) bimetallic nanocomposite material is higher than that of Pd NPs ($4.254e^{-7}$).

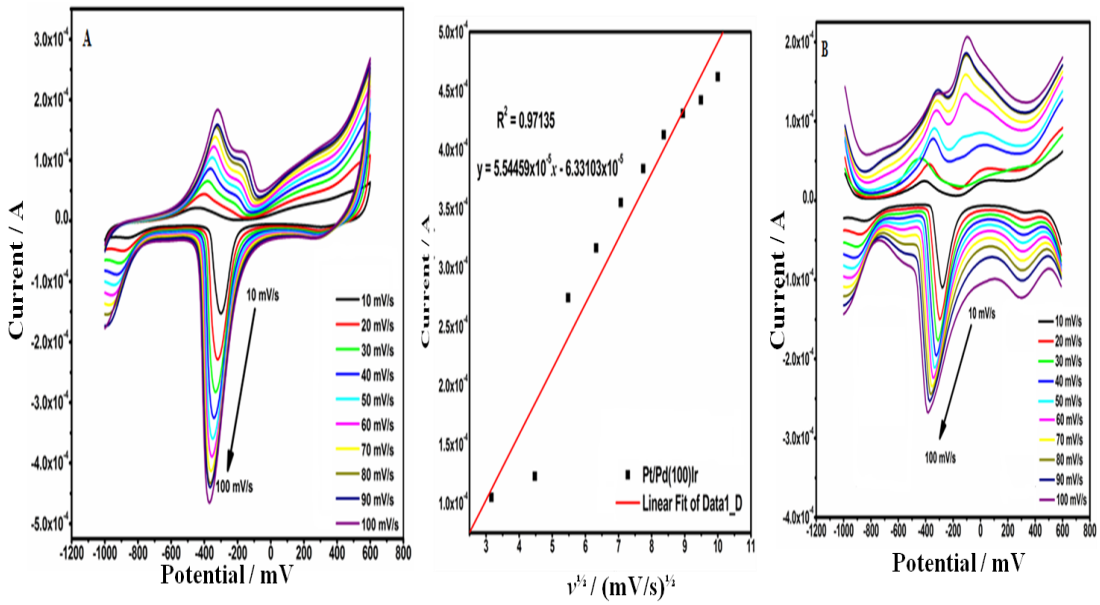

Figure 6. CV (A) and SWV (B) of modified Pt electrode with Pd(100)Ir in 0.1 M NaOH at different scan rates; and the Randles-Sevčik plot.

3.7 Electrochemical study of Pd NPs and Pd(100)Ir by electrochemical impedance spectroscopy (EIS) technique

EIS was used to investigate the interfacial properties of the Pt/Pd NPs and Pt/Pd(100)Ir electrodes and the results obtained were analyzed using Nyquist and Bode plots. The Nyquist plot in Fig. 7 (A) demonstrated a semi-circle and a Warburg diffusion line which is an indication that the electrochemical process on the electrode surface is kinetically controlled at higher frequencies and diffusion controlled at lower frequencies [22-24]. These results revealed that the bimetallic nanocomposite {Pd(100)Ir} has smaller charge transfer resistance (R_{ct}) values compared to the monometallic nanoparticles {Pd NPs} These findings are due to the combination of two different metals within the composite with increased kinetics of charge transfer reaction at the metal interface when compared to the monometallic nanoparticles. The charge transfer resistance is a measure of the resistance associated with the electron transfer process and is inversely related to the exchange current density. A low R_{ct} indicates a facile interfacial electron transfer process and hence a higher specific pseudo-Faradaic capacitance [23-25]. The EIS results are in a good agreement with the results obtained from CV (Fig. 5) where the bimetallic nanocomposite {Pd(100)Ir} illustrated high peak current density values which are seen as lower charge transfer resistance values in EIS. The parameters determined from EIS results were, R_{ct} = 880.90 Ω and R_s = 219.7 Ω which represent the charge transfer resistance and solution resistance resulting from modified Pt electrode with the Pd NPs, whereas the Pt electrode modified with the bimetallic nanocomposite {Pd(100)Ir} (red curve) showed a decrease in the charge

transfer resistance (R_{ct} = 110.67 Ω and R_s = 140 Ω). This drop in R_{ct} can be attributed to the excellent activity and good conductivity of these nanomaterials; thus, making them highly suitable for charge transfer applications and also indicating that they have better electron transfer kinetics. An equivalent circuit model was developed to fit the impedance parameters. [22, 26].

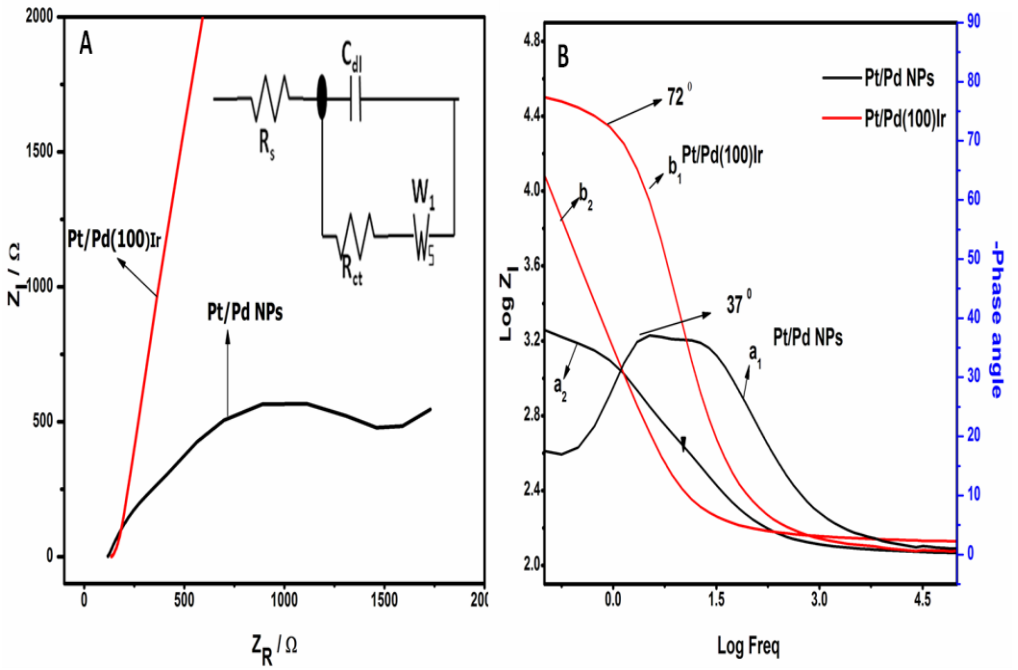

Figure 7. Nyquist plot (A) and Bode plot (B) of Pt electrode modified with Pd NPs {black line} and Pd(100)Ir {red line} in 0.1 M NaOH solution.

The circuit elements were used to calculate the time constant and the exchange current using Equation 3.4. The results revealed that electrode modification with the monometallic nanoparticles {Pd NPs} gave lower exchange current and higher time constant values (9.6889 x 10^{-2} A, 6.3241 x 10^{-4} s /rad), while the inverse was observed for the bimetallic nanocomposites {Pd(100)Ir} (2.3193 x 10^{-1} A, 2.6728 x 10^{-7} s /rad).

$$R_{ct} = RT/nFi_0 \qquad (3.4a)$$

$$i_o = \frac{RT}{nFR_{ct}} \qquad (3.4\ b)$$

$$\omega_{max} = 2\pi f = \frac{1}{R_{ct}C_{dl}} \qquad (3.4\ c)$$

$$\tau = R_{ct}C_{dl} \qquad (3.4\ d)$$

Where n is the number of electrons transferred, i_0 is the standard exchange current (A), C_{dl}. is the double layer capacitance and τ is the time constant. The other parameters have their usual meanings.

The Bode plots in Fig. 7 (B) provided information on the impedance, frequency and phase angle. Maximum phase angles of 72 ° and 37 ° were obtained for Pd(100)Ir and Pd NPs respectively. These findings show the Bode phase angle of the bimetallic nanocomposites to be very close to 90 ° which is an indication of a higher metallic conductivity. These findings were corroborated by the Nyquist plot in Fig. 7 A where lower charge transfer resistance values were observed for the bimetallic nanocomposites.

4. ELECTROCHEMICAL OXIDATION OF AMMONIA

4.1 Electrochemical oxidation of ammonia on Pt/Pd(100)Ir electrode

Fig. 8 represents the cyclic and square wave voltammograms of unmodified and modified platinum electrode with Pd(100)Ir in 0.1M NaOH solution containing ammonia. In Fig. 8 (A and B), the black curve observed was for unmodified Pt electrode in 0.1M NaOH solution containing ammonia.

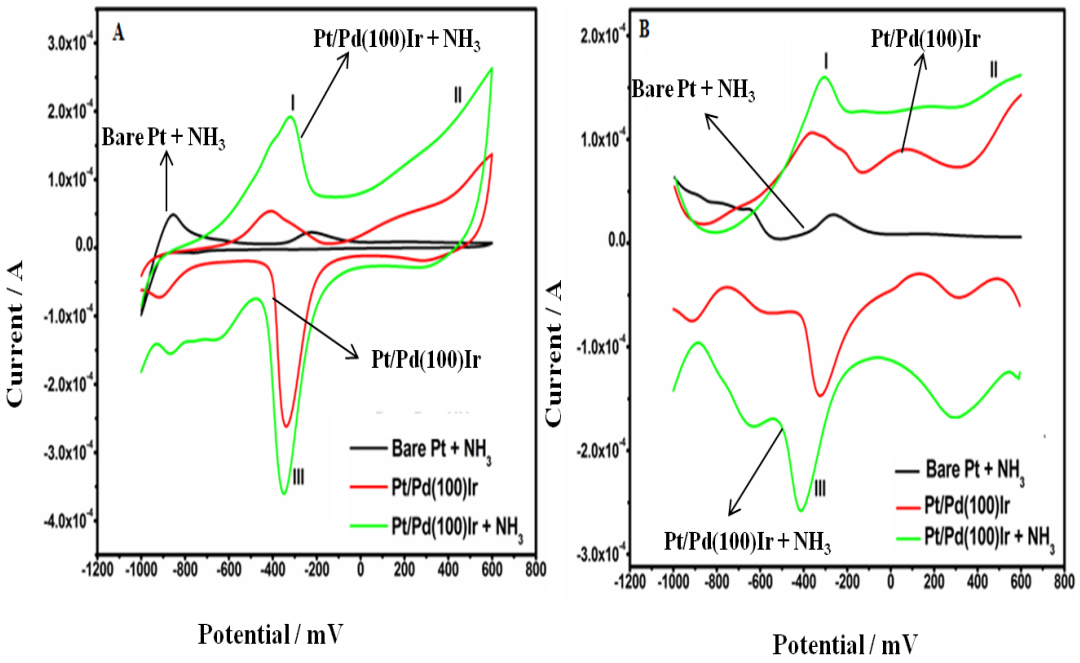

Figure 8. CV (A) and SWV (B) characterization of unmodified and modified platinum electrode with Pd(100)Ir in. 0.1 M NaOH solution containing ammonia and ammonia-free solution at a scan rate 50 mV/s.

A small anodic potential peak at ≈ - 0.2 V (Peak I) was observed in the presence of ammonia, and corresponds to ammonia oxidation [27]. This indicates that platinum electrode can oxidize ammonia. The observed voltammetric response of the modified platinum electrode in the absence of ammonia is depicted in Fig. 8 (red curve) where a strong reduction peak was observed at around the potential ≈ -0.4 V, attributed to the reduction of Pd(II) oxide into elemental Pd. The green curve shows

the Pd(100)Ir modified platinum electrode in the NaOH solution containing ammonia where an anodic peak at around ≈ -0.4 V (peak I) was identified due to the oxidation of ammonia. A cathodic current peak at around ≈ -0.4 to ≈- 0.6 V (peak III) was also observed and this resulted from the reduction of Pd^{2+} to Pd^{0}. The observed voltammetric response of Pt/Pd(100)Ir illustrated that the onset of oxidation and reduction (Peak I and III) shifted to a more negative potential and the high current density is probably due to a catalyzing effect of the transition metal catalysts on the platinum electrode.

4.2 The effect of ammonia concentration on the electrocatalytic activity of modified platinum electrode

Fig 9 (A and B) shows the CV and line graph of Pt/Pd NPs and Pt/Pd(100)Ir in 0.1 M NaOH solution containing different concentrations of ammonia. When different ammonia concentrations were added to the solution, the peak current density at peak III corresponding to reduction of Pd and peak I corresponding to ammonia oxidation starts rising steadily due to the release of H^{+} during ammonia oxidation and reaches a maximum where a decrease occurs resulting from Pd surface deactivation by strongly adsorbed nitrogen (N_{ads}) because they block the catalytic active sites [5, 28]. As the ammonia concentration increases, the ammonia adsorbate is dissociated then dehydrogenated to NH_{2ads}, with N_2 produced [5]. Maximum peak current density from Fig. 9 was plotted as a function of ammonia concentration (Fig. 9 B).This observation may be due to the fact that the rate of N_{ads} formation increases with concentration therefore, blocking active sites of the Pt electrode surface and preventing ammonia electrooxidation [5]. The electrode surface may also be saturated with different adsorbed species, hence affecting the ability of the catalyst to oxidize at higher concentrations of ammonia [5]. Peak current density decrease with increase in ammonia concentration may be due to the poisoning of electrode surface by inert N_{ads}.

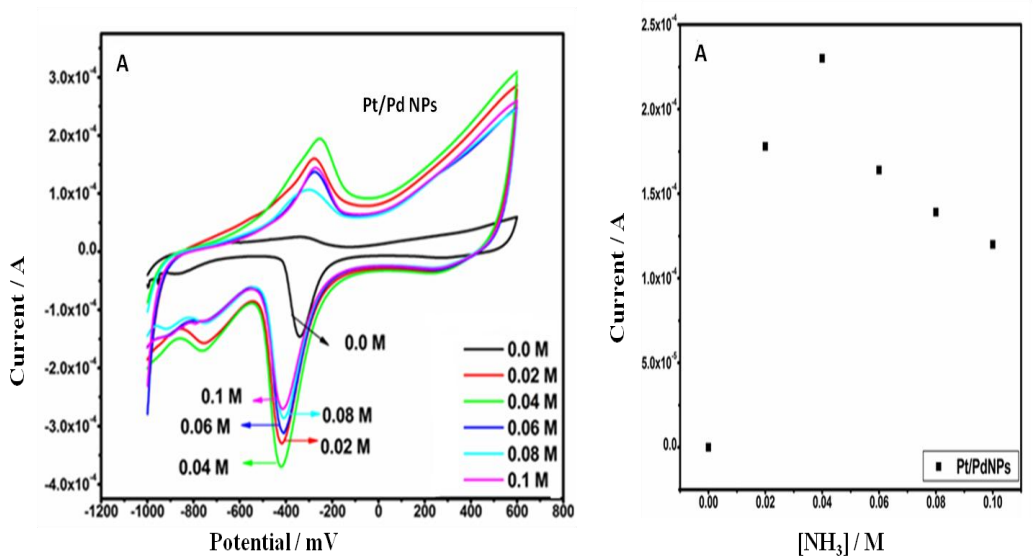

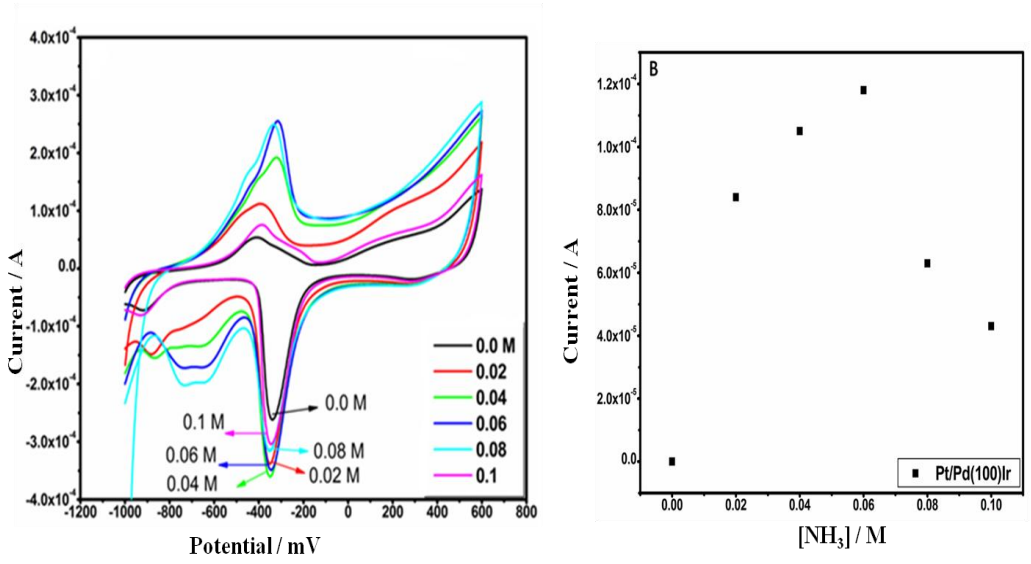

Figure 9. Cyclic voltammogram and line graph of modified platinum electrode with Pd NPs (A) and Pd(100)Ir (B) in 0.1 M NaOH solution containing different concentrations of ammonia at a scan rate 50 mV/s.

4.3 Comparison of the electrochemical behaviour of modified platinum electrode with Pd NPs, and Pd(100)Ir towards ammonia oxidation

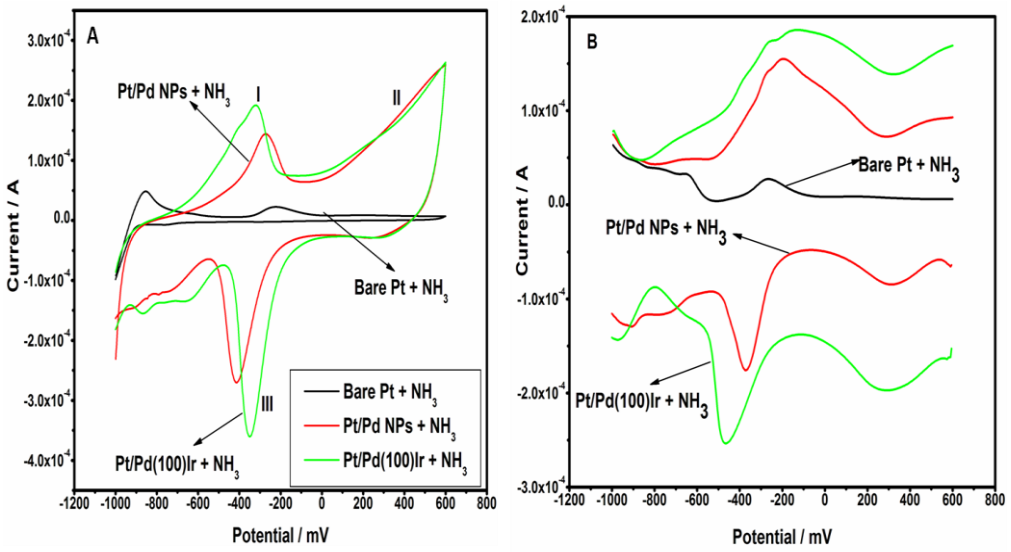

Figure 10. CV (A) and SWV (B) characterization of unmodified and modified platinum electrodes with Pd NPs and Pd(100)Ir in. 0.1 M NaOH solution containing ammonia at a scan rate 50 mV/s.

Fig. 10 (A and B) shows the CV and SWV of Pt/Pd NPs (red curve) and Pt/Pd(100)Ir (green curve) in an ammonia-containing solution. From this analysis, the Pd(100)Ir and Pd NPs showed excellent voltammetric responses towards ammonia oxidation. The Pd(100)Ir exhibited a higher catalytic activity and good conductivity towards ammonia oxidation than the Pd NPs. The catalytic

activity was proved by the sharp increase in peak current and reached a maximum for the NH_3 oxidation at 1.9838 x 10^{-4} A whereas the Pd NPs maximum was at about 1.45 x 10^{-4} A. The higher catalytic activity of the bimetallic electrode was also demonstrated by the decreased onset potential for ammonia oxidation at -0.7 V while the Pd NPs had onset potential at – 0.4 V. This was also proved by calculating the electrochemical active surface area (EASA) which revealed that Pd(100)Ir has a higher electrochemical active surface area when compared to Pd NPs (83.02 and 58.73 cm^2 respectively). Based on these results, having bimetallic Pt/Pd(100)Ir has advantages in the catalytic activity for ammonia electrooxidation due to a cooperative interaction between Pd- and Ir-containing catalysts, causing weakening of the adsorption strength of poisonous N_{ads} intermediate [5].

4.4 Electrochemical study of Pd NPs and Pd(100)Ir by Electrochemical Impedance Spectroscopy Technique (EIS)

4.4.1 Nyquist plot analysis

The Nyquist plot in Fig 11 (A) illustrated that the bimetallic nanocomposites {Pd(100)Ir} has smaller R_{ct} values compared to the monometallic nanoparticles {Pd NPs}. The parameters obtained by the fitting analysis are presented in Table 1 for the monometallic nanoparticles {Pd NPs} and bimetallic nanocomposites {Pd(100)Ir}. The immobilization of bimetallic nanocomposites {Pd(100)Ir} on the electrode surface led to a decrease in the semicircle diameter in the impedance spectra with a corresponding decrease in the R_{ct} values.

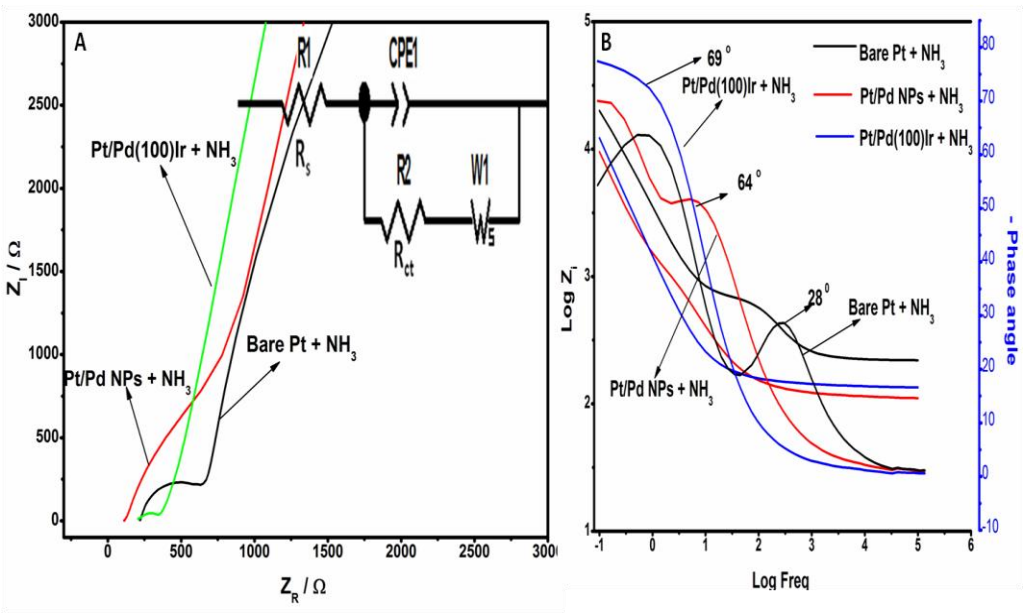

Figure 11. Nyquist plot (A) and Bode plot (B) of the unmodified Pt electrode (black line) and the modified electrode with Pd NPs (red line) and Pd(100)Ir (green line) in 0.1 M NaOH containing ammonia solution and the equivalent circuit.

These EIS results are in a good agreement with the results obtained from the cyclic and square wave voltammograms (Fig. 10) where the bimetallic nanocomposites {Pd(100)Ir} illustrated higher current density values which are seen as lower charge transfer resistance values in EIS. The findings are also in good agreement with literature where it has been suggested that bimetallic nanocomposites show enhanced catalytic properties than monometallic nanoparticles [29].

Further EIS analyses revealed that electrode modification by the monometallic nanoparticles {Pd NPs showed lower exchange current (i_0) values and higher time constant values while the inverse was observed for the bimetallic nanocomposites {Pd(100)Ir}. The results indicate that the electrode modified with the bimetallic nanocomposites improved the kinetics at the electrode surface compared to the monometallic nanoparticles. This highly agrees with findings reported in various literatures that the use of bimetallic nanocomposite catalysts enhance reaction kinetics. An equivalent circuit model was developed to fit the impedance parameters [22, 25]. The parameters were used to calculate the time constant and the exchange current and tabulated in Table 2.

Table 1. Circuit parameters obtained from the fitting analysis

electrode	R_s / Ω	R_{ct} / Ω	Z_w
Pt/Pd(100)	189.5	670.6	103,71
Pt/Pd(100)Ir	137.9	96.35	191.02

Table 2. Kinetic parameters

	Kinetic parameters	
	Exchange current	Time constant
Pt/Pd(100)	3.8252 e^{-2}A	9.4126e^{-4} s /rad
Pt/Pd(100)Ir	2.6624 e^{-1}A	2.0539e^{-7} s /rad

5. CONCLUSION

Palladium nanoparticles (Pd NPs) and palladium(100)iridium bimetallic nanocomposite {Pd(100)Ir} were synthesized and their electrocatalytic properties for ammonia oxidation evaluated. CV and SWV techniques showed the bimetallic nanocomposite {Pd(100)Ir} to have better conductivity and higher catalytic activity towards the electrochemical oxidation of ammonia. The

superiority of the bimetallic electrocatalyst was validated by the maximum current density reached for NH_3 oxidation where it gave a value of 1.9838 x 10^{-4} A with a decreased onset potential. The Pd NPs showed reduced catalytic activity at 1.45 x 10^{-4} A. EIS results further confirmed that facile interfacial electron transfer processes occur with the bimetallic nanocomposite and is thus considered an excellent electrocatalyst for electrode materials in the production of hydrogen which is an attractive alternative clean fuel generated from NH_3 decomposition and is applicable in fuel cells.

ACKNOWLEDGEMENTS
The research work was financially supported by the National Research Foundation (NRF), South Africa and the University of the Western Cape.

References

1. S. L. Vot, L. Roué and D. Bélanger, *J. Electroanal. Chem*., 691 (2013) 18.
2. C. M. Hung, *Int. J. Hydrogen Energy*, 37 (2012) 13815.
3. N. J. Bunce and D. Bejan, *Electrochim. Acta*, 56 (2011) 8085.
4. A. Kapalka, S. Fierro, Z. Frontistis, A. Katsaounis, S. Neodo, O. Frey, N. de Rooij, K. M. Udert and C. Comninellis, *Electrochim. Acta,* 56 (2011) 1361.
5. T. L. Lomocso and E. A. Baranova, *Electrochim. Acta*, 56 (2011) 8551.
6. A. Allagui, M. Oudah , X. Tuaev, S. Ntais, F. Almomani and E. A. Baranova, *Int. J. Hydrogen Energy*, 38 (2013) 2455.
7. A. Kapalka, A. Cally, S. Neodo, C. Comninellis, M. Wachter and K. M. Udert. *Electrochem. Commun.*, 12 (2010) 18.
8. F. J. Vidal-Iglesias, J. Solla-Gullon, V. Montiel, J. M. Feliu and A. Aldaz. *J. Power Sources*, 171 (2007) 448.
9. N. Seirafianpour, S. Badilescu, Y. Djaoued, R. Brüning, S. Balaji, M. Kahrizi and V. V. Truong, *Thin Solid Films*, 516 (2008) 6359.
10. G. Asimellis, N. Michos, I. Fasaki and M. Kompitsas, *Spectrochim. Acta, Part B: Atomic Spectroscopy*, 63 (2008) 1338.
11. L. L. Thegy and A. B. Elena, *Electrochim. Acta*, 56 (2011) 8551.
12. T. Soundappan, F.Y. Rong and C. Shen-Ming, *Int. J. Electrochem. Sci*., 6 (2011) 4537.
13. C. L. Lee, H. P. Chiou and C. R. Liu, *Int. J. Hydrogen Energy*, 37 (2012) 3993.
14. J. Mingshang, L. Hongyang, Z. Hui, X. Zhaoxiong, L. Jingyue and X. Younan, *Nano Res*, 4 (2011) 83.
15. G. J. M. Dille and S. Godet, *Nanomed. J*., 8 (2012) 37.
16. D. S. Sheny, D. Philip and J. Mathew, *Spectrochim. Acta, Part A: Molecular and Biomolecular Spectroscopy*, 91 (2012) 35.
17. M. Meena Kumari, S.A. Aromal, and D. Philip, *Spectrochim. Acta Part A: Molecular and Biomolecular Spectroscopy*, 103 (2013) 130.
18. F. Wang, S. Tang, H. Ma, L. Wang, X. Li and B. Yin, *Chin. J. Chem.*, 32(2014) 1225.
19. R. Rosa, A. M. Ferraria, A. M. B. do Rego and M. C. Oliveira, *Electrochim. Acta*, 87 (2013) 73.
20. Z. X. Liang, T. S. Zhao, J. B. Xu and L. D. Zhu, *Electrochim. Acta*, 54 (2009) 2203.
21. S. Zhirong, H. Yanbo, G. Ming, W. Xuefeng and H. Xiang, *Int. J. Electrochem. Sci*., 6 (2011) 5626.
22. C. O. Ikpo, N. Njomo, K. I. Ozoemena, T. Waryo, R. A. Olowu, M. Masikini, A. A. Baleg, N. Jahed, P. G.L. Baker and E. I. Iwuoha, *Nano Hybrids*, 3 (2013) 1.
23. X. Yang, F. Zhang, Y. Hu, D. Chen, Z. He and L. Xiong, *Int. J. Electrochem.Sci.*, 9 (2014) 5061.

24. C. Wan, L. Yuan and H. Shen *Int. J. Electrochem.Sci.,* 9 (2014) 4024.
25. R. Ramya, R. Sivasubramanian and M.V. Sangaranarayanan, *Electrochem. Acta*, 101 (2013) 109.
26. L. Wu, J. Liu, M. Yu, S. Li, H. Liang, and M. Zhu, *Int. J. Electrochem. Sci.,* 9 **(**2014) 5012
27. A. D. Luis, V. M. Ana, M. Madhivanan and G.B. Gerardine, *Electrochim. Acta*, 89 (2013) 413.
28. V. C. Arnau, H. F. Patricia, E. L. S. Ifan and S. D. Chorkendorff, *J. Power Sources*, 220 (2012) 205.
29. F. Albert, D. C. Riccardo, M. Liberato and P. Teresa *Pharmacol. Res.,* 62 (2010) 126.